Fuzzy Connectedness Image Co-segmentation for Hybrid PET/MRI and PET/CT Scans

Ziyue Xu, Ulas Bagci, Jayaram K. Udupa and Daniel J. Mollura

Abstract In this paper, we presented a 3-D computer-aided co-segmentation tool for tumor/lesion detection and quantification from hybrid PET/MRI and PET/CT scans. The proposed method was designed with a novel modality-specific visibility weighting scheme built upon a fuzzy connectedness (FC) image segmentation algorithm. In order to improve the determination of lesion margin, it is necessary to combine the complementary information of tissues from both anatomical and functional domains. Therefore, a robust image segmentation method that simultaneously segments tumors/lesions in each domain is required. However, this task, named co-segmentation, is a challenging problem due to (1) unique challenges brought by each imaging modality, and (2) a lack of one-to-one region and boundary correspondences of lesions in different imaging modalities. Owing to these hurdles, the algorithm is desired to have a sufficient flexibility to utilize the strength of each modality. In this work, seed points were first selected from high uptake regions within PET images. Then, lesion boundaries were delineated using a hybrid approach based on novel affinity function design within the FC framework. Further, an advanced extension of FC algorithm called iterative relative FC (IRFC) was used with automatically identified background seeds. The segmentation results were compared to the reference truths provided by radiologists. Experimental results showed that the proposed method effectively utilized multi-modality information for co-segmentation, with a high accuracy (mean DSC of 85 %) and can be a viable alternative to the state-of-the art joint segmentation method of random walk (RW) with higher efficiency.

U. Bagci (✉)
Center for Research in Computer Vision (CRCV), HEC 221, Computer Science,
University of Central Florida, Orlando, FL 32816, USA
e-mail: bagci@crcv.ucf.edu

Z. Xu · D.J. Mollura
Center for Infectious Disease Imaging, Radiology and Imaging Sciences
National Institutes of Health, Bethesda, MD 20892, USA

J.K. Udupa
Department of Radiology, University of Pennsylvania,
Philadelphia, PA 19104, USA

F. Gao et al. (eds.), *Computational Methods for Molecular Imaging*,
Lecture Notes in Computational Vision and Biomechanics 22,
DOI 10.1007/978-3-319-18431-9_2

Keywords Co-segmentation · Fuzzy connectedness · PET/MRI · PET/CT · Image segmentation

1 Introduction

Multimodal imaging techniques make use of different but complementary imaging modalities within a single system. While PET/CT sequentially acquires computed tomography (CT) and positron emission tomography (PET) images from a patient, PET/MRI simultaneously acquires PET and magnetic resonance (MR) images, and provides very accurate spatial and temporal image fusion. With PET/MRI and PET/CT, the spatial distribution of radiotracer activity from PET can be precisely analyzed with anatomical details revealed by MRI or CT, leading to more accurate localization and characterization of pathology. PET/MR and PET/CT have thus emerged as a mean of achieving higher sensitivity and specificity than either component modality alone. Most automated tumor/lesion segmentation methods are either solely based on PET images and ignore complementary MRI or CT information, or vice versa. Lately, the requirements for joint analysis of lesions in both structural and functional image domains led researchers to develop co-segmentation methods for robust quantification of lesions [1, 2].

In this paper, as an alternative to the state-of-the-art methods, we propose an efficient framework for hybrid imaging modalities segmentation. Our proposed method is based on a fuzzy connectedness (FC) image segmentation [3], which effectively utilizes a modality-specific visibility weighting scheme through a novel fuzzy affinity function. Our method is flexible to withstand various visibility conditions of the object of interest in different modalities. In clinical routines, high uptake regions of radiotracers in PET images are usually determined by the visual assessment of radiologists based on the fused information. This process is labor intensive and time consuming. Thresholding, edge detection, region growing, and watershed approaches have also been employed to determine the region boundaries [4], but these algorithms were developed solely on functional images without incorporating anatomical information. Therefore, the methods are limited in accuracy, robustness, and reproducibility. Recently, a few co-segmentation methods have been proposed for quantification of PET/CT images [1, 2, 5, 6]. Feature extraction and classification, considering both PET and CT information for distinguishing tumor from normal tissue in the head and neck regions, is presented in [5]. In [6], localization and initial segmentation were performed over PET images, which is further refined by voxel classification in CT. The above methods [5, 6] are based on classification, which lack the capability of concurrent segmentation from both modalities. Markov Random Field (MRF) model was employed for PET/CT co-segmentation in [1]; graph optimization was performed to simultaneously minimize the total MRF energy obtained from both PET and CT images. The MRF-based method was shown to be effective; however, it works on a 2-D slice plane and requires a precisely defined seed set provided by user interaction. In [2], random walk (RW) co-segmentation was applied to find the correct anatomical

boundaries in CT images, driven by the uptake regions from the corresponding PET images. The RW-based algorithm was shown to perform better than MRF in both accuracy and speed. In this paper, we propose an alternative method to these state-of-the-art methods [1, 2]. An automatic 3-D co-segmentation method was designed based on the FC framework with a novel fuzzy affinity function. Our method has the flexibility to segment tumors/lesions jointly through a modality-specific weight mechanism; experiments have been conducted on images from hybrid PET/MRI and PET/CT scans.

2 Methods

In this section, the theory of FC is presented, followed by co-segmentation formulation.

In the FC framework, a fuzzy topological construct characterizes how voxels of an image hang together to form an object through a predefined function called *affinity* [7]. Assuming $\mathcal{V} \subset \mathbb{Z}^3$ denotes a 3-D cubic grid representing the *image space*, where each element of $\mathcal{V}$ is called a *voxel*, a topology on an image is given in terms of an *adjacency* relation (μ_α). Theoretically, if p and q are α-adjacent to each other, then $\mu_\alpha(p, q) = 1$, '0' otherwise. In practice, we set $\alpha = 26$ for 3-D analysis. While affinity is intended to be a local relation, a global fuzzy relation called fuzzy connectedness, is induced on the image domain by the affinity functions. This is done by considering all possible paths between any two voxels p and q in the image domain, and assigning a strength of fuzzy connectedness to each path. The level of the fuzzy connectedness between any two voxels p and q is considered to be the maximum of the strengths of all paths between p and q.

An *affinity relation* κ is the most fundamental measure of local hanging togetherness of nearby voxels. For a path π, which is a sequence of voxels $\langle p_1, p_2, \ldots, p_l \rangle$ with every two successive voxels being adjacent, given *fuzzy affinity function* $\mu_\kappa(p_i, p_{i+1})$, the strength of the path is defined as the minimum affinity along the path:

$$\mu_{\mathcal{N}}(\pi) = \min_{1 \le i < l} \mu_\kappa(p_i, p_{i+1}). \tag{1}$$

Then, the strength of connectedness $\mu_{\mathcal{K}}(p, q)$ between any two voxels p and q is the strength of the strongest path between them as

$$\mu_{\mathcal{K}}(p, q) = \max_{\pi \in \mathcal{P}(p,q)} \mu_{\mathcal{N}}(\pi), \tag{2}$$

where $\mathcal{P}(p, q)$ denotes the set of all paths between p and q. Therefore, a fuzzy connected object $\mathcal{O}$ in an image can be defined for a predetermined set of seeds S. Since the level of FC between any two voxels p and q is considered to be the maximum of the strengths of all paths between them, for multiple seeds, the fuzzy object membership function for $\mathcal{O}$ or the strength of connectedness of $\mathcal{O}$ is defined

as follows:

$$\mu_{\mathcal{O}}(p) = \max_{s \in S} \mu_{\mathcal{K}}(p, s). \tag{3}$$

An efficient computational solution is presented in [3] for computing $\mu_{\mathcal{O}}(p)$, given κ and S and an image.

Absolute FC segmentation is based on computing the FC strength between a set of seed points and all other voxels within the image and set a proper threshold to the resulting FC image for generating the binary segmentation result. However, the threshold determination is usually manual. On the other hand, IRFC method is based on several seed sets $S_i, i = 1, 2, \ldots, k$. FC strength is first computed at every voxel for each of the seed sets individually, and then the voxel is labeled as belonging the seed set with maximum FC value. In this way, the thresholding step is avoided. In this study, we investigated both the application of FC and IRFC.

2.1 Image Co-segmentation with Novel Affinity Function

Effectiveness of the FC/RFC algorithm depends on the choice of the affinity function. The most prominent affinities used so far are (i) adjacency-based μ_α, (ii) homogeneity-based μ_ψ, and (iii) object feature-based μ_ϕ such that fuzzy affinity is defined as

$$\mu_\kappa(p, q) = \begin{cases} 1, & \text{if } p = q; \\ \mu_\alpha(p, q)\sqrt{\mu_\psi(p, q)\mu_\phi(p, q)}, & \text{otherwise,} \end{cases} \tag{4}$$

where $\mu_\psi(p, q)$ captures the homogeneity between p and q, with a higher value for similar pairs. For object feature-based affinity, $\mu_\phi(p, q)$ defines the hanging-togetherness of p and q in the target object based on likeliness of their feature values with respect to the expected feature distribution of the target object. The general form of $\mu_\psi(p, q)$ and $\mu_\phi(p, q)$ are

$$\mu_\psi(p, q) = e^{-\frac{|f(p)-f(q)|^2}{2\sigma_\psi^2}}, \tag{5}$$

$$\mu_\phi(p, q) = \min\left(e^{-\frac{|f(p)-m|^2}{2\sigma_\phi^2}}, e^{-\frac{|f(q)-m|^2}{2\sigma_\phi^2}}\right), \tag{6}$$

where σ_ψ and σ_ϕ are two different standard deviation parameters used for homogeneity and object feature distribution, m is the mean object feature value, and f denotes image intensity function: $f : \mathcal{V} \to \mathcal{L} \subset \mathbb{Z}$.

In order to introduce a co-segmentation framework, we introduce two intensity functions corresponding to anatomical ($\mathcal{A}$: MRI or CT) and functional ($\mathcal{F}$: PET)

image domain, $f^{\mathcal{A}}$ and $f^{\mathcal{F}}$, respectively. Similarly, for each image modality $\mathcal{A}$ and $\mathcal{F}$, we define a new fuzzy affinity function by combining fuzzy affinity functions corresponding to anatomical and functional images (i.e., $\mu_\kappa^{\mathcal{A}}(p,q)$ and $\mu_\kappa^{\mathcal{F}}(p,q)$) as

$$\mu_\kappa(p,q) = \begin{cases} 0, & \text{if } \mu_\kappa^{\mathcal{A}}(p,q) \text{ or } \mu_\kappa^{\mathcal{F}}(p,q) = 0; \\ w_{\mathcal{A}}\mu_\kappa^{\mathcal{A}}(p,q) + w_{\mathcal{F}}\mu_\kappa^{\mathcal{F}}(p,q), & \text{otherwise;} \end{cases} \tag{7}$$

where weights $w_{\mathcal{A}}$ and $w_{\mathcal{F}}$ are used to combine affinities, and were determined by considering target visibility of different modalities such that they were constrained as $0 \leq w_{\mathcal{A}}, w_{\mathcal{F}} \leq 1$, and $w_{\mathcal{A}} + w_{\mathcal{F}} = 1$.

We also designed a new object feature-based affinity function specific to the image modality by analyzing the characteristics of individual imaging modalities. A non-uniform Gaussian formulation was utilized for this purpose. The functions designed for this purpose are illustrated in Fig. 1. As can be seen from the first row of the figure that since the *hot* regions are more active for a PET image, thus inferring more reliable target volume, we can define an expected value m from the image intensity distribution that shapes the non-uniform Gaussian formulation as

$$\mu_\phi^{\mathcal{F}}(x) = \begin{cases} 1, & \text{if } f^{\mathcal{F}}(x) > m; \\ e^{-\frac{|f^{\mathcal{F}}(x)-m|^2}{2\sigma_\phi^2}}, & \text{otherwise.} \end{cases} \tag{8}$$

In a similar fashion, to model the object feature-based affinity function, higher and lower intensity variations can be combined with respect to an object feature as

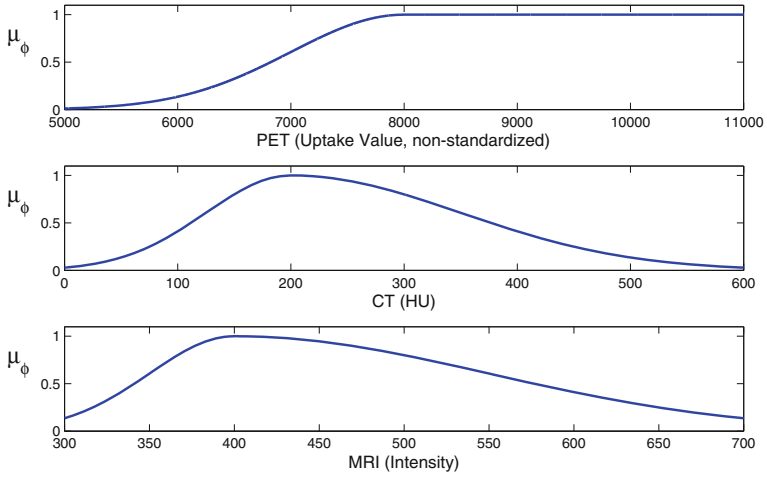

Fig. 1 Non-uniform Gaussian formulation for object feature similarity μ_ϕ

$$\mu_{\phi}^{\mathcal{A}}(x) = \begin{cases} e^{-\frac{|f^{\mathcal{A}}(x)-m|^2}{2\sigma_{\phi_{\mathrm{H}}}^2}}, & \text{if } f^{\mathcal{A}}(x) > m; \\ e^{-\frac{|f^{\mathcal{A}}(x)-m|^2}{2\sigma_{\phi_{\mathrm{L}}}^2}}, & \text{otherwise,} \end{cases} \tag{9}$$

where $\sigma_{\phi_{\mathrm{L}}} < \sigma_{\phi_{\mathrm{H}}}$. Second and third rows in Fig. 1 demonstrate the object feature-based affinity functions used for CT and MRI modalities, respectively. Once all affinity functions were defined, Eq. 3 was solved to obtain segmentation results.

3 Experiments and Results

Data and Evaluation Metrics: A retrospective study was performed on 9 PET/MRI and 9 PET/CT images. For comparison with the state-of-the-art algorithm of RW [2], we have used **the same dataset, reference segmentation, and evaluation criterion**. For PET/MRI scans, voxel sizes were $1.1 \times 1.1 \times 6$ mm^3 for MR images and $4.17 \times 4.17 \times 2$ mm^3 for PET images. For PET/CT scans, voxel sizes were $0.97 \times 0.97 \times 1.5$ mm^3 for CT images and $2.65 \times 2.65 \times 3$ mm^3 for PET images. Each patient's scan was positive for at least one mass tumor in the neck, thorax, abdomen, or pelvis pertaining to Von Hippel-Lindau disease, pheochromocytoma, or hereditary leiomyomatosis and renal cell cancer, as previously identified (but not circumscribed) by a radiologist. Manual delineations from two expert observers on PET/CT and PET/MR images were used as reference for evaluation, and the segmentation performance was evaluated using two conventional segmentation metrics, the Dice Similarity Coefficient (DSC) and Hausdorff Distance (HD). Note that DSC calculates the ratio of overlap between two segmentation results and HD measures the boundary mismatch between two segmentations. Higher DSC and lower HD are desirable for a segmentation algorithm. Seed points are manually determined, and variations are allowed given that FC is the most robust method for seed selection [8].

3.1 Qualitative and Quantitative Evaluation

The experiments were conducted on a machine with 2.7 GHz CPU, 16GB memory, and Mac OS X system. Average running time for the proposed co-segmentation algorithm was less than 10 seconds. RFC doubles the time complexity of FC, and we found no statistical significant difference between FC and IRFC results regarding segmentation accuracy. Figure 2 shows examples of the co-segmentation results from PET/MR images under different visibility conditions of the target object. The second column displays the fused images overlaid by segmentation results (green boundaries) and manual references (blue boundaries). The first and the third columns show corresponding PET and MR images. As illustrated, the visibility of the target object and contrast with surrounding tissues are more prominent in PET for the first row (showing a small tumor); the target object is almost equally visible for the second row

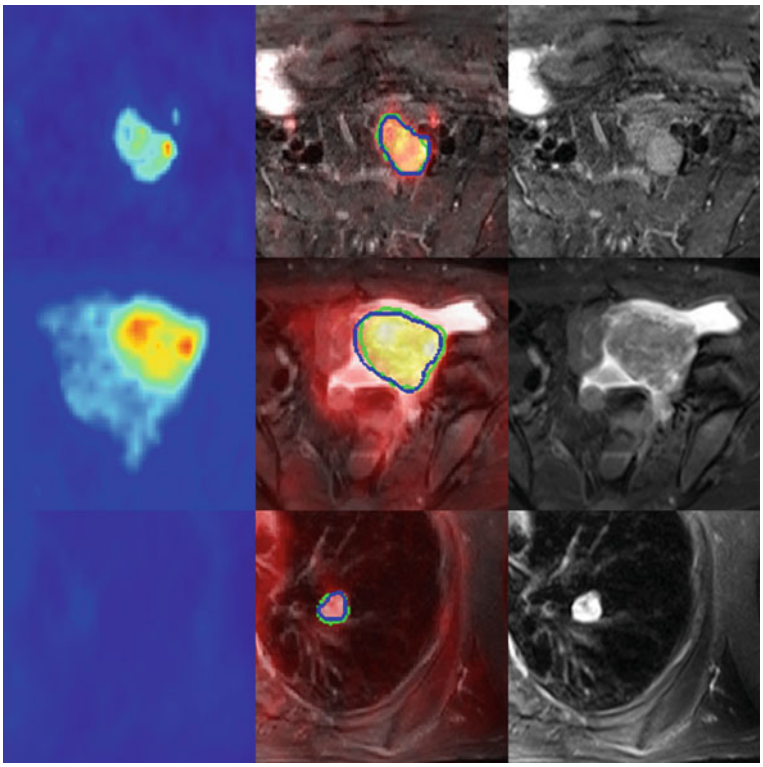

Fig. 2 Co-segmentation results for PET/MR images under different visibility conditions. *The first column* PET images in three different anatomical levels. *The second column* hybrid PET/MR image with segmentation results (*green contours*) and manual references (*blue contours*) overlaid. *The third column* corresponding MR images. Target object is more visible in PET for the first row (*small tumor*); almost equally visible for the second row (*big tumor*); and more visible in MRI for the third row (lung mass)

(showing a larger tumor); and the target object is more prominent in MRI for the third row (showing lung mass). Qualitatively, the co-segmentation results agree well with the anatomical boundaries, as well as hot regions from functional images. Similarly, results for PET/CT images are qualitatively presented in Fig. 3. The second column is the fused images overlaid by segmentation results (green boundaries) and manual references (blue boundaries). The first and the third columns are corresponding PET and CT images. The first row illustrates a consolidation case where the contrast between consolidation region and surrounding tissue in CT image is subtle for the human eye, as pointed out by the red arrow (consolidation) and the yellow arrows (blood vessels). The second row presents a tree-in-bud case where the contrast is higher, but the infected region contains complex structures in the CT image. As can be observed, when contrast between the target region and the surrounding tissue is subtle, human observers tend to rely more on the PET image, while the automatic algorithm is able to capture the difference in both images. Note that in the

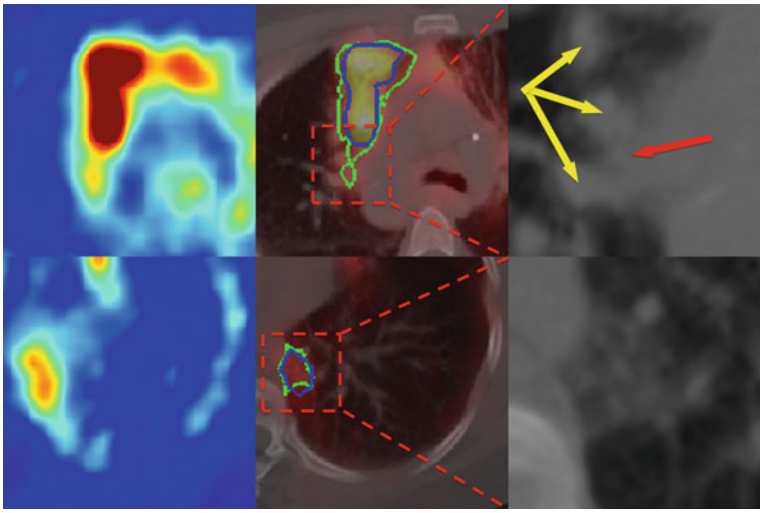

Fig. 3 Co-segmentation results for two PET/CT images. *The first column* PET images in two different anatomical levels. *The second column* hybrid PET/CT image with segmentation results (*green contours*) and manual references (*blue contours*) overlaid. *The third column* corresponding CT images. Contrast between target region and surrounding tissue is subtle for the first row (consolidation), as pointed out by the *red arrow* (consolidation) and the *yellow arrows* (blood vessels), differentiating vessels and consolidations is almost impossible visually. Target region has higher contrast but contains complex structures in the second row (tree-in-bud)

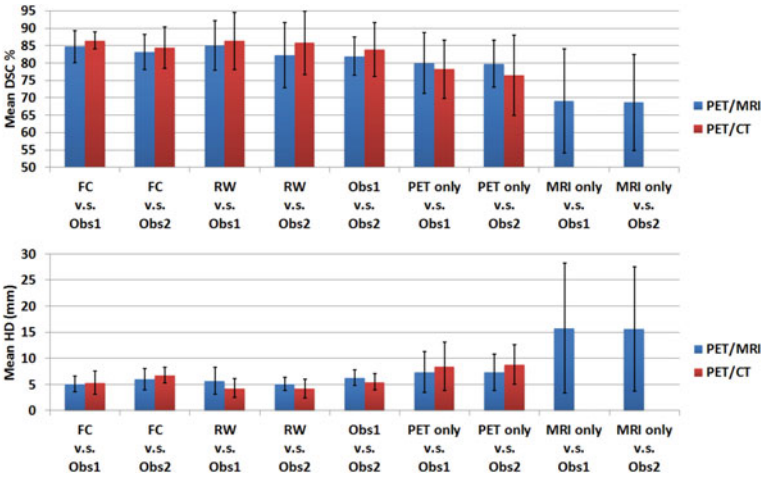

Fig. 4 DSCs and HDs for segmentation results, given by different methods and manual delineations

CT images in Fig. 3, the target object is only partially defined by lung and is discriminant from the surrounding soft tissues with subtle contrast; therefore, segmentation solely based on CT images is often not feasible for the experimental data. Mean and standard deviation of the delineations' DSCs and HDs are presented in Fig. 4. As illustrated, co-segmentation on PET/MR and PET/CT images helps to improve the results over MRI, CT, or PET alone, and it performs better than or comparable to inter-observer variation. Also, although CT alone has poor intensity resolution and gives partial description of the target object, it helps to improve the segmentation with additional boundary constraint.

4 Discussion and Conclusion

In this paper, we proposed a co-segmentation framework using both anatomical and functional images. The proposed method was performed in 3-D image domain, with flexibility to segment various lesions under different visibility conditions. The performance of the method was evaluated using PET/MR and PET/CT images, and high accuracy was achieved. In comparison with the RW image co-segmentation [2], which achieves a DSC of 86 %, our proposed method had a similar performance with heightened efficiency; therefore, our method can be an alternative to the state-of-the-art method. Indeed, the proposed framework performs delineation of the lesions about four times faster than the RW co-segmentation method. Note that perfect registration is assumed for the input anatomical and functional images, and proper registration is needed in presence of mismatches. Also, motion correction could be applied before segmentation to account for inter- and intra-scan motions during imaging. These two issues are important factors for the final accuracy, although they are out of the scope of the proposed framework. Furthermore, it will be meaningful in our future work to test the proposed method on heterogeneous tumors considering the strength of FC in handling variations of local image intensities.

Acknowledgments This research is supported by CIDI, the intramural research program of the National Institute of Allergy and Infectious Diseases (NIAID) and the National Institute of Biomedical Imaging and Bioengineering (NIBIB).

References

1. Han, D., Bayouth, J., Song, Q., Taurani, A., Sonka, M., Buatti, J., Wu, X.: Globally optimal tumor segmentation in PET-CT images: a graph-based co-segmentation method. Inf. Process. Med. Imaging **22**, 245–256 (2011)
2. Bagci, U., Udupa, J.K., Mendhiratta, N., Foster, B., Xu, Z., Yao, J., Chen, X., Mollura, D.J.: Joint segmentation of anatomical and functional images: applications in quantification of lesions from PET, PET-CT, MRI-PET, and MRI-PET-CT images. Med. Image Anal. **17**(8), 929–945 (2013)

3. Udupa, J.K., Samarasekera, S.: Fuzzy connectedness and object definition: theory, algorithms, and applications in image segmentation. CVGIP **58**(3), 246–261 (1996)
4. Drever, L., Robinson, D., McEwan, A., Roa, W.: A comparison of three image segmentation techniques for PET target volume delineation. J. Appl. Clin. Med. Phys. **8**(2), 93–109 (2007)
5. Yu, H., Caldwell, C., Mah, K.: Coregistered FDG PET/CT-based textural characterization of head and neck cancer for radiation treatment planning. IEEE Trans. Med. Imaging. **28**(3), 374–383 (2009)
6. Potesil, V., Huang, X., Zhou, X.S.: Automated tumor delineation using joint PET/CT information. In: SPIE Med. Imaging (2007)
7. Saha, P.K., Udupa, J.K.: Fuzzy connected object delineation: axiomatic path strength definition and the case of multiple seeds. Comput. Vis. Image Underst. **83**(3), 275–295 (2001)
8. Ciesielski, K., Udupa, J., Falco, A., Miranda, P.: Fuzzy connectedness image segmentation in graph cut formulation: a linear-time algorithm and a comparative analysis. J. Math. Imaging Vis. **44**(3), 375–398 (2012)

http://www.springer.com/978-3-319-18430-2

Computational Methods for Molecular Imaging
Gao, F.; Shi, K.; Li, S. (Eds.)
2015, VII, 205 p. 72 illus., 54 illus. in color., Hardcover
ISBN: 978-3-319-18430-2